# PHASE DISTRIBUTION IDENTIFICATION IN THE COLUMN LEACHING OF LOW GRADE ORES USING MRI

**Authors**

M.A. Fagan [a]

maf52@cam.ac.uk

A.J. Sederman [a *]

ajs40@cam.ac.uk

S.T.L. Harrison [b]

Sue.Harrison@uct.ac.za

M.L. Johns [c]

michael.johns@uwa.edu.au

[a] Department of Chemical Engineering and Biotechnology, University of Cambridge, Pembroke Street, Cambridge, CB2 3RA, UK

Tel: +44 1223 766338

Fax: +44 1223 334796

[b] Centre for Bioprocess Engineering Research, Department of Chemical Engineering, University of Cape Town, Rondebosch, 7701, South Africa

[c] School of Mechanical and Chemical Engineering, University of Western Australia, 35 Stirling Highway, Crawley, WA 6009, Australia

* Corresponding author

## ABSTRACT

Heap bioleaching is gaining importance as an approach for the recovery of valuable metals (e.g. $Cu^{2+}$) from low grade ores. In this process iron and/or sulfur oxidising microorganisms are used to aid the oxidation of base metal sulfides in the ore, thereby liberating the metal ions into solution. Leach performance is strongly influenced by the contacting of the leach solution and the ore particles. In order to better understand the distribution of the leaching solution on the pore scale in these heaps, Magnetic Resonance Imaging (MRI) was used to acquire images non-invasively of a section of an irrigated ore bed. This was made possible by the use of specialist MRI acquisition sequences suited to the magnetically heterogeneous environment as presented by the ore material. From the images we were able to determine the pore-occupancy of the liquid and gas phases and to provide novel measurement of the interfacial area between air, leach solution and ore.



**Keywords**

MRI, Heap leaching, Hydrometallurgy, Interfacial area, Process optimisation

# 1 INTRODUCTION

In recent decades heap bioleaching has become an established method for the extraction of copper and other base metals from low grade ore (Brierley, 2008). The growth in the importance of bioleaching has lead to a greatly improved understanding of the processes and microorganisms involved. Still, there are a number of challenges associated with heap leaching in general, many of which are the result of the sheer size of the heaps combined with their inhomogeneous nature. This study focuses on the issue of heap hydrology, with a specific interest in how the liquid is distributed through the packed ore.

Solution flow in heaps needs to be fast enough to ensure that leaching occurs in an economically feasible time period, while the flow must also be sufficiently uniform that areas of the heap are not left unleached. However, heaps are unsaturated systems of often highly inhomogeneous nature which makes the hydrology of the leaching systems complex and spatially variable, leading to issues such as flooding and preferential flow (O'Kane Consultants Inc., 2000). Most of the studies done on heap hydrology have adopted a macroscopic approach via analysis of heap feed and effluent and have focussed primarily on the issue of preferential flow and on the development of models to predict heap hydrodynamics. The research group of Lin and Miller took a microscopic experimental approach, using X-ray computed tomography (CT) to image leaching systems before and after leaching (Lin *et al.*, 2005). X-ray CT however provides limited signal contrast between the air and liquid phases in the presence of comparatively high density solids. In the context of bioleaching X-ray radiation could also sterilise the column. Hence complementary methods for real time imaging and analysis of the liquid flow in leaching systems are desirable.

The application of Magnetic Resonance Imaging (MRI) to heap leaching has the potential to provide additional measurement capability by acquiring 3D images of the liquid in an ore-packed column non-invasively as a leach progresses. It can readily differentiate between air and water, as signal is only detected from the water. MRI would not typically be thought of as a viable tomographic technology for use with such ores because the high concentration of ferro- and para-magnetic species in the ore and leach solution may cause significant image distortions due to magnetic susceptibility

gradients and other physical effects. It has been found that such image distortions can be minimised through the use of Spin Echo Single Point Imaging (SESPI), a specialist MRI acquisition sequence (Ouriadov *et al*., 2004). In a previous study we have shown via direct, unambiguous comparison with X-ray CT images of saturated ore beds that the SESPI technique is compatible with the ore material used and is able to provide accurate and hence quantitative images (Fagan *et al*., 2012). This compatibility with the ore is largely because the spatial dependence of the signal is phase encoded during SESPI and thus measurement of the time evolution of the signal (as is the case for conventional MRI pulse sequences) is avoided. As a result, the extent to which chemical shift, magnetic susceptibility and dipolar and quadrupolar image distortions are observed is significantly reduced, a phenomenon that is described in detail in Gravina and Cory (1994).

The aim of the current study is to use SESPI to acquire images of a flowing, partially saturated ore column. These images are used with images of a fully flooded column to produce a 3D phase map to illustrate the relative positions of the gas, liquid and solid phases within the column. This map is used subsequently to quantify various parameters characterising the system hydrodynamics including holdup, contact between phases and distribution of phases with respect to the solid matrix.

## 2 MATERIALS AND METHODS

### 2.1 Leaching column

Low grade copper ore was used in the experiments. It had an average composition of 2.95% Fe, 0.69% Cu and 2.02% S on a weight basis. The particle size distribution, measured by sieving, is given in Table 1. The ore (400 g) was agglomerated with 20 ml of 0.1 M sulfuric acid and packed into the column illustrated in Figure 1. The inner diameter of the column was 50 mm which was restricted by the magnet's internal bore. The total height of the ore bed was 135 mm and the gravimetric voidage of the packed ore was found to be 38.5±0.8%. Distilled water was used for the liquid phase. The column was irrigated drip-wise from the top at a rate of 40 ml $h^{-1}$ during the main flowing experiment as well as at 20 ml $h^{-1}$ and 60 ml $h^{-1}$. This is approximately equivalent to 10, 20 and 30 L $m^{-2}$ $h^{-1}$. The system was allowed two hours to stabilise

before any images were acquired, at which point the outlet flow rate matched the inlet. For the flooded images, water was used to fully saturate the bed.

**Table 1**

Particle size distribution for the ore used in the leaching column

| Size (mm) | Weight (%) |
|---|---|
| > 13.2 | 13.9 |
| 13.2 – 9.5 | 18.4 |
| 9.5 – 5.6 | 20.3 |
| 5.6 – 2.0 | 19.8 |
| 2.0 – 0.71 | 9.1 |
| < 0.71 | 18.5 |

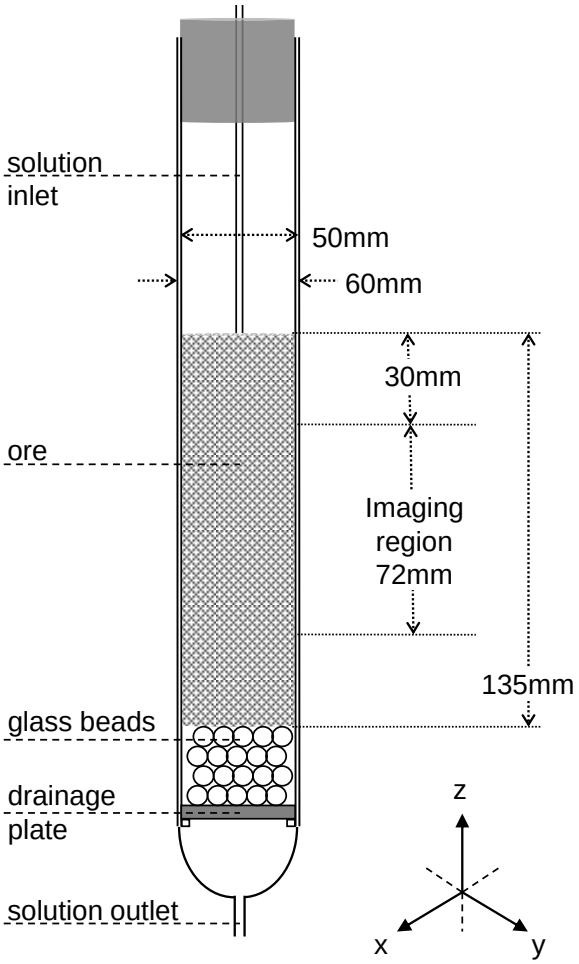


**Figure 1.** Schematic of the leaching column with the ore bed and imaging region heights indicated.

### 2.2 Magnetic resonance imaging

Imaging was conducted on a Bruker DMX 200 4.7 T vertical-bore spectrometer with an RF coil with internal diameter of 63 mm and an imaging region of approximately 70 mm in length. A single echo per excitation SESPI pulse sequence with split phase-encoding gradients was used. Further details can be found in Fagan *et al*. (2012). The field of view was 60 mm × 60 mm in the horizontal plane (x and y) and 72 mm in the vertical direction (z). The acquisition size was 64×64×32, which corresponded to a resolution of 938 μm in the horizontal plane and 2250 μm in the vertical plane. The resolution was limited by the maximum allowable gradient strengths and time restrictions. The acquisitions had a repeat time (*TR*) of 50 ms, a total gradient encoding time ($t_p$) of 350 μs and an echo time (*TE*) of 870 μs. Four repeat scans were done for phase cycling and eight points were acquired along the echoes and added together in order to improve the final signal to noise ratio (SNR).

## 3 RESULTS AND DISCUSSION

### 3.1 Production of phase map

Since signal in the MRI images is obtained only from the liquid phase, the flooded column images could be used to identify the void space within the column whilst the flowing images only showed where the solution was present in the partially saturated system. The positions of the solid, liquid and gas phases could therefore be identified by combining the two acquisitions to produce a 3D phase map (Sederman and Gladden, 2001). Figure 2a shows a representative 2D slice (from the 3D image) of the flooded column, binary gated to liquid (white) and solid ore (black) in Figure 2b. The corresponding slice for the unsaturated 40 ml $h^{-1}$ flowing system is shown in Figure 2c with the binary gated image shown in Figure 2d (here black indicates solid ore or air). By addition of Figure 2b and d we produced Figure 2e, a phase map where white represents the gas phase, grey is the liquid phase and black is the solid ore phase or outside the sample. In the phase map we had to account for partial volume effects where pixels are occupied by more than one phase. They were identified as those pixels that were assigned to be non-void (solid) pixels in the flooded image gating, but were subsequently identified as being occupied by liquid in the flowing system images. It was not possible to determine what fraction of these pixels was liquid filled, therefore two boundary scenarios were considered for the calculation of the various phase

distribution properties. In the one case the partial volume pixels were assumed to be liquid filled, thereby allowing for an upper bound to be calculated. The pixels were assumed to be free of liquid in the lower bound scenario. The 3D phase map is shown in Figure 3 with air (white), water (light and dark grey for filled and partially filled pixels) and solid (black) identified. For clarity of presentation we show corresponding 2D slices in Figure 4, extracted from the 3D image in the axial direction where the separation distance is 2250 μm.

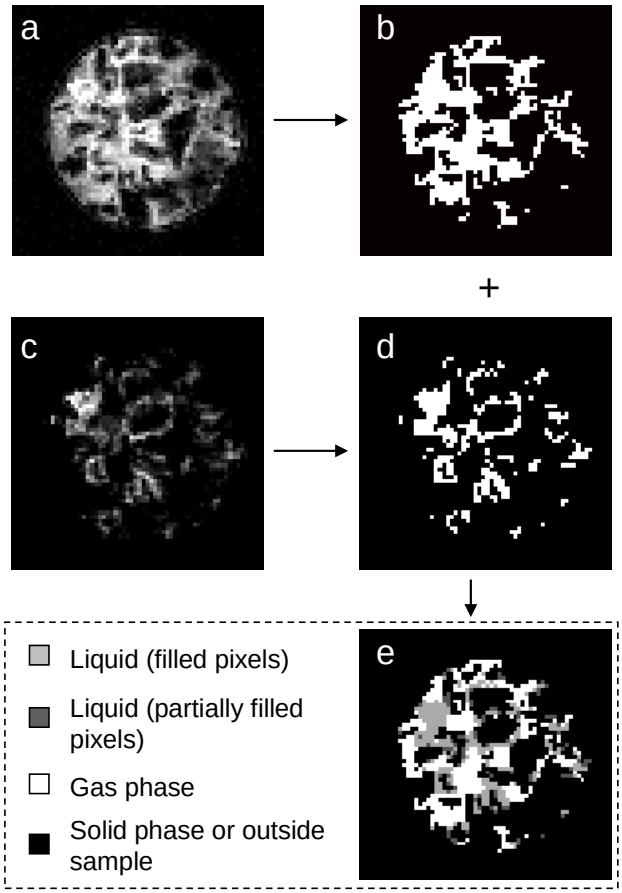


**Figure 2.** Processing of the MRI data to produce the phase map. The (a) flooded column images are thresholded to (b) binary images. The same is done for the (c) flowing column images to produce (d). The thresholded images (b) and (d) are finally combined to produce the phase map (e).

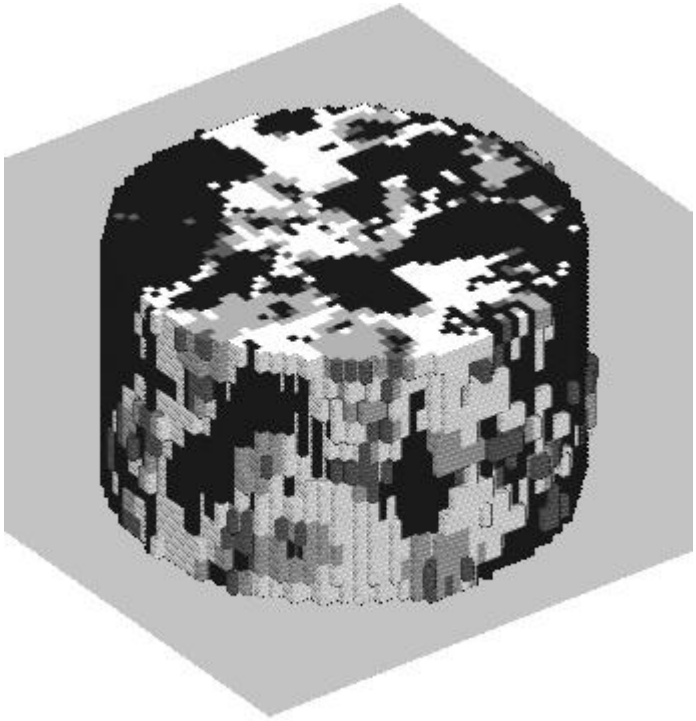

**Figure 3.** Full 3D phase map of the unsaturated column after data analysis as described in the text. Different shades of grey are used to identify the various phases as shown in Figure 2e.

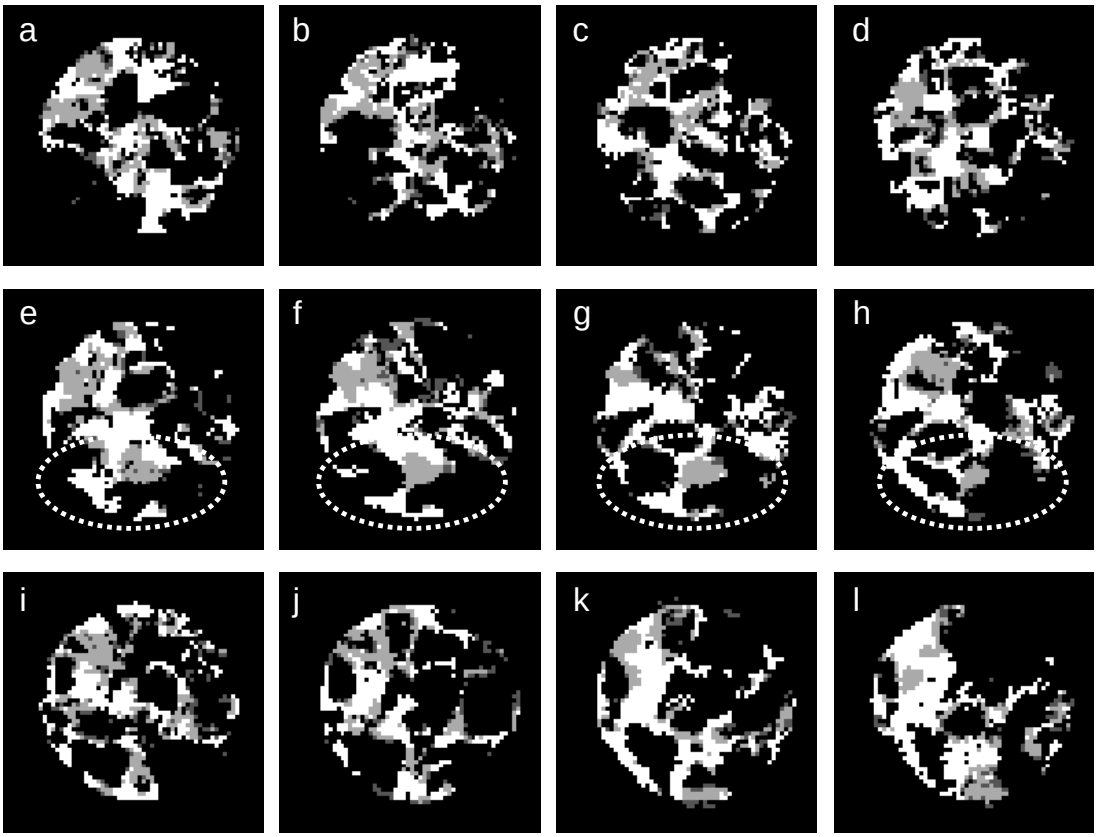


**Figure 4.** 2D phase maps of the unsaturated column extracted from the 3D data shown in Figure 3. The slices have an axial separation of 2250 μm where (a) is at the top of the imaging region and (l) is at the bottom. Different shades of grey are used to identify the various phases as shown in Figure 2e. Interlinking flow channels are highlighted in slices (e) to (h).

The average voidage of the imaging region was estimated to be 41.7±2.4% from the flooded image. The error margins, determined according to the variation within the sample, overlapped with the gravimetrically determined voidage of 38.5±0.8%. Direct agreement is not expected as the gravimetric measurement was necessarily performed on the whole ore sample. For the unsaturated flowing column, the liquid phase was calculated to account for 17.4±2.2% and the gas phase accounted for 24.4±2.4% of the total bed space. These overall and phase-specific values are in good agreement with those reported previously in the heap leaching literature. For example in Bouffard and Dixon (2001), their columns had an average total void fraction of 43% and the most similar columns to the one studied here had a liquid content of between 12 and 23% which compares favourably to the circa 17% measured here. They determined these

values using standard gravimetric measurements and by measuring effluent flow volumes.

An additional set of experiments was done where the column was operated with flow rates of 20 ml $h^{-1}$, 40 ml $h^{-1}$ and 60 ml $h^{-1}$. The liquid holdup in the imaging region was calculated from the gated images. It was found to increase from 15.7% to 16.7% to 17.0% respectively. This result from the thresholded images is supported by the fact that the signal intensity at the centre of **k**-space (MRI signal acquisition domain) increased with flow rate, a result which is indicative of an increase in liquid holdup.

The flow paths of the liquid were also observed to change in some places in the column. An example of this is shown in Figure 5, where the flow paths in this slice are seen to change between flow rates. In particular, new rivulets are seen to form as has been predicted by Ilankoon and Neethling (2012) as well as previously observed in trickle beds at low flow rates (Sederman and Gladden, 2001).

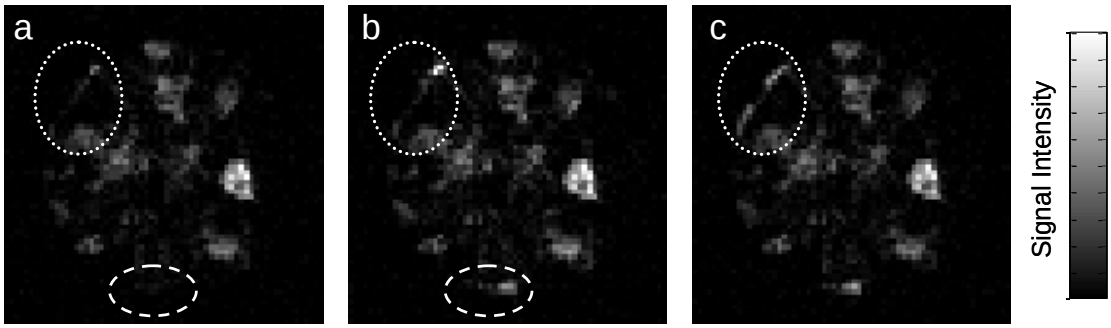


**Figure 5.** 2D slices of the flowing column when irrigated at a rate of (a) 20 ml $h^{-1}$, (b) 40 ml $h^{-1}$ and (c) 60 ml $h^{-1}$. New rivulets that developed with the flow rate changes are highlighted.

### 3.2 Column wetting

Different types of flow could be observed from the phase maps. With respect to Figure 4, channels of flow are evident linking adjacent slices, such as in the bottom half of images e - h (highlighted). The majority of the solution was seen to flow along the edges of the ore particles in thin films or between adjacent particles as pore flow, where pores refer to an inter-particle phenomenon. This is consistent with the ore being preferentially water-wetting. The phase maps were used to determine the distance of the

liquid from a solid edge boundary in order to explore this observation quantitatively. This was done using the pore thinning algorithm of Baldwin *et al*. (1996) on the total void space after which the liquid pixels were identified. The results are given in Table 2.

It was found that 57.8±5.4% of the liquid occurred less than 1 mm from the solid while only 2.5±0.4% was located more than 3 mm from a solid boundary. The effect of considering the partial volume pixels to be liquid filled was to increase the number of total void and liquid pixels nearest the surface, resulting in a larger percentage range for those pixels less than 1 mm from the solid. This was expected as the partial volume effect is defined as being between the liquid and the solid phases. Furthermore, the percentage of the void space occupied by liquid for the larger distance ranges remains approximately constant at around 40%. This indicates that not all flow was dominated by wettability effects and that some liquid flow was in the form of larger channels.

**Table 2**

Position of the liquid in the column expressed as its distance from the solid surface and the percentage of the void space at that distance. The error measurements are generated by considering partial volume effects.

| Distance from solid boundary (mm) | % of liquid pixels | % of void space occupied by liquid |
|---|---|---|
| < 1 | 57.8 ± 5.4 | 39.6 ± 6.0 |
| 1 – 2 | 26.1 ± 3.1 | 38.1 ± 0.9 |
| 2 – 3 | 13.7 ± 1.9 | 34.5 ± 0.5 |
| 3 – 4 | 1.7 ± 0.3 | 44.3 ± 0.2 |
| 4 – 5 | 0.7 ± 0.1 | 41.8 ± 0.0 |
| 5 – 6 | 0.1 ± 0.0 | 40.0 ± 0.0 |

An alternative approach to the distance calculation is to generate the distance map from the liquid pixels only and not the total void space. This takes into account that the liquid may not be connected to the nearest solid surface by other liquid pixels. For the majority of the liquid (77%) the distance is unchanged from the distances that were populated for Table 2. For the remaining pixels the liquid film bridged beyond the centre of the pore, whilst not making contact with the other side, resulting in a longer distance to the solid. The maximum liquid film thickness in the bed was determined to be 7.3 mm using this method. This measurement of liquid film thickness is important with respect to the mass transfer of oxygen and carbon dioxide from the gas to the

leaching sites. The average distance of the liquid from a solid edge was calculated using the second method to be 1.22–1.31 mm, compared with 1.37 mm for the total void space. This confirms that overall the liquid slightly favoured high surface flow in the form of small pore rivulets, a behaviour that may be attributed to wettability effects.

### 3.3 Interfacial area between phases

The phase maps allow for the measurement of the interfacial area between the different phases. The gas-liquid interfacial area for the column was determined to be 906±57 $m^2$ $m^{-3}$ of liquid. The volume of column considered excluded the pixels adjacent to the column walls to avoid including wall effects in the analysis. This value also refers to the entire liquid volume as the stagnant and flowing liquid were not individually identified.

Previous ore leaching studies have found that the rate limiting step in heap bioleaching is gas-liquid mass transfer (Petersen, 2010a; Petersen, 2010b) with the supply of oxygen as well as carbon dioxide to the liquid phase reaction systems becoming mass transfer limited. The rate of gas adsorption ($r_{GLMT}$) is usually modelled as

$$r_{GLMT} = k_L a\left(c^* - c_b\right) \quad (1)$$

where $k_L a$ is the lumped area-mass transfer coefficient, $c^*$ is the solubility of the gas at the gas-liquid interface and $c_b$ is the bulk concentration within the liquid. The mass transfer coefficient has been treated in the literature as this lumped parameter as it can be determined experimentally from exit measurements (Petersen, 2010a). Values reported in the bioleaching literature range between 20 and 47 $h^{-1}$ (Bouffard and Dixon, 2009; Petersen, 2010a; Petersen and Dixon, 2007). The coefficient is a combination of $k_L$, the overall gas-liquid mass transfer coefficient (m $h^{-1}$), with $a$, the available gas-liquid contact area per unit volume of stagnant solution ($m^2$ interfacial area/$m^3$ liquid). The gas-liquid contact area has not been measured separately for such leaching systems, though its effect has been indirectly discussed in the literature with respect to the influence of particle size distribution on the magnitude of $k_L a$ (Petersen, 2010a). Measurement of $a$ using MRI would allow for the factors which affect $a$ to be examined. This would enable the best design and operation of a leach to be identified with respect to the maximisation of the gas-liquid interfacial area and consequently the optimisation gas-liquid mass transfer.

The liquid-solid interfacial area is an indicator how much of the ore's surface is available for leaching. It was found to be 389±42 $m^2$ $m^{-3}$ solid. The gas-solid interfacial area was found to be 576±91 $m^2$ $m^{-3}$ solid. Therefore less than half of the ore's exposed surface area was in contact with liquid. If this system was leached with the current flow pattern it is thus possible that the majority of the metal would not be recovered, a problem that has been seen in the industrial operation of heaps (O'Kane Consultants Inc., 2000).

The relatively coarse spatial resolution of the MRI images and the SNR will have had an effect on the accuracy of these results. Finer details in the structure are not accounted for and will cause an artificial reduction in the surface area, whilst the pixilation of the interface will cause an increase in the measured surface area. Furthermore, very thin films of liquid may have been unaccounted for in the distance measurements and liquid-solid contact area. These sources of error could be minimised in future experiments by using a higher imaging resolution. However, any resolution improvements would depend on the magnet capabilities and the degree to which it is necessary to acquire undistorted images.

## 4 CONCLUSIONS

This study has shown that it is possible to use MRI to image heap leaching systems under flowing conditions, despite the para- and ferro-magnetic metal content of the ore. The images were used to produce a 3D map of phase distribution, from which the solid, liquid and gas phase positions could be identified quantitatively. The voidage of the imaging region calculated from the phase map was 41.7±2.4% which compared well with the gravimetrically determined overall voidage of 38.5±0.8%. The liquid and gas phases were found to account for 17.4±2.2% and 24.4±2.4% respectively of the total bed space under flowing conditions at 40 ml $h^{-1}$. All of these values compare favourably with those presented in the literature. It was found that of the liquid in the column, 57.8±5.4% occurred less than 1 mm from a solid boundary, with the average distance of the liquid from a solid edge between 1.22 and 1.31 mm. Only 2.5±0.4% of the liquid was more than 3 mm from a solid edge. It was also demonstrated that the different phase contact areas could be measured using the phase map. The gas-liquid interfacial

area was found to be 906±57 $m^2$ $m^{-3}$ liquid. Less than half of the solid surface was in contact with liquid which is likely to lead to inefficient leaching of the ore.

Future experiments of the type presented here could have implications on the understanding of the distribution of liquid between the stagnant and flowing phases in a variety of leaching systems. Coupling MRI experiments like this one with more traditional hydrodynamics experiments such as tracer studies (Bouffard and Dixon, 2001; Bouffard and West-Sells, 2009; De Andrade Lima, 2006) and the techniques described by Bouffard and Dixon (2001) to measure flowing and stagnant liquid are therefore now being pursued and could help validate these leaching hydrodynamic descriptions.

## ACKNOWLEDGEMENTS

The authors would like to acknowledge and thank the University of Cape Town, BHP Billiton and the Cambridge Commonwealth Trust for their sponsorship and support of this project.

## REFERENCES

Baldwin, C.A., Sederman, A.J., Mantle, M.D., Alexander, P. and Gladden, L.F., Determination and characterization of the structure of a pore space from 3D volume images. Journal of Colloid and Interface Science, 1996, 181 (1), 79-92.

Bouffard, S.C. and Dixon, D.G., Investigative study into the hydrodynamics of heap leaching processes. Metallurgical and Materials Transactions B - Process Metallurgy and Materials Processing Science, 2001, 32 (5), 763-776.

Bouffard, S.C. and Dixon, D.G., Modelling pyrite bioleaching in isothermal test columns with the HeapSim model. Hydrometallurgy, 2009, 95 (3-4), 215-226.

Bouffard, S.C. and West-Sells, P.G., Hydrodynamic behavior of heap leach piles: Influence of testing scale and material properties. Hydrometallurgy, 2009, 98 (1-2), 136-142.

Brierley, C.L., How will biomining be applied in future? Transactions of Nonferrous Metals Society of China, 2008, 18 (6), 1302-1310.

De Andrade Lima, L.R.P., Liquid axial dispersion and holdup in column leaching. Minerals Engineering, 2006, 19 (1), 37-47.

Fagan, M.A., Sederman, A.J. and Johns, M.L., MR imaging of ore for heap bioleaching studies using pure phase encode acquisition methods. Journal of Magnetic Resonance, 2012, 216 (1), 121-127.

Gravina, S. and Cory, D.G., Sensitivity and resolution of constant-time imaging. Journal of Magnetic Resonance Series B, 1994, 104 (1), 53-61.

Ilankoon, I.M.S.K. and Neethling, S.J. Hysteresis in unsaturated flow in packed beds and heaps. Minerals Engineering, 2012, 35 (1), 1-8.

Lin, C.L., Miller, J.D. and Garcia, C., Saturated flow characteristics in column leaching as described by LB simulation. Minerals Engineering, 2005, 18 (10), 1045-1051.

O'Kane Consultants Inc., Demonstration of the application of unsaturated zone hydrology for heap leaching optimization, Industrial Research Assistance Program Contract # 332407. O'Kane Consultants Inc., Saskatoon, 2000.

Ouriadov, A.V., MacGregor, R.P. and Balcom, B.J., Thin film MRI - high resolution depth imaging with a local surface coil and spin echo SPI. Journal of Magnetic Resonance, 2004, 169 (1), 174-186.

Petersen, J., Determination of oxygen gas-liquid mass transfer rates in heap bioleach reactors. Minerals Engineering, 2010a, 23 (6), 504-510.

Petersen, J., Modelling of bioleach processes: Connection between science and engineering. Hydrometallurgy, 2010b, 104 (3-4), 404-409.

Petersen, J. and Dixon, D.G., Modeling and optimization of heap bioleach processes. In *Biomining* ed. D.E. Rawlings and B.D. Johnson. Springer-Verlag, 2007, pp. 153-176.

Sederman, A.J. and Gladden L.F., Magnetic resonance imaging as a quantitative probe of gas–liquid distribution and wetting efficiency in trickle-bed reactors. Chemical Engineering Science, 2001, 56 (8), 2615-2628.